Spin-orbital entangled two-dimensional electron gas at the LaAlO_{3}/Sr_{2}IrO_{4} interface

Churna Bhandari and S. Satpathy

Phys. Rev. B **98**, 041303 — Published 20 July 2018

DOI: 10.1103/PhysRevB.98.041303

Spin-orbital entangled 2DEG at the $LaAlO_3/Sr_2IrO_4$ interface

Churna Bhandari and S. Satpathy
Department of Physics and Astronomy, University of Missouri, Columbia, MO 65211, USA

Using density-functional studies, we show that a spin-orbital entangled two-dimensional electron gas (2DEG) forms at the (001) $LaAlO_3/Sr_2IrO_4$ polar interface between an ordinary band insulator and a spin-orbit coupled Mott insulator, aided by the combination of the spin-orbit coupling, Coulomb interaction, and polar catastrophe. Quite remarkably, the 2DEG is found to be localized on a single IrO_2 monolayer, unlike other polar interfaces such as $LaAlO_3/SrTiO_3$, where the 2DEG is several monolayers thick. The electron gas occupies the upper J_{eff}=1/2 Hubbard band in the interface layer, which becomes half-filled with a simple square-like Fermi surface. If successfully grown, this would be the first candidate material to host the spin-orbital entangled 2DEG.

PACS numbers: 73.20.-r, 75.70.Tj

In a seminal paper, Ohtomo and Hwang[1] reported the observation of a conducting layer of 2DEG at the interface between two 3d transition metal oxides, $LaAlO_3$ (LAO) and $SrTiO_3$ (STO), that led to an explosion of research in this area and the discovery of a number of exotic phenomena at the oxide interfaces such as the giant negative magnetoresistance[2], interfacial magnetism, which can be controlled by charge leakage[3] or by gate voltage[4], tunable Rashba spin-orbit interaction,[5] and the coexistence of magnetism[6] and superconductivity.[7] It has been suggested that the interface may be a candidate material for Majorana fermions[8] and may even host the ever-elusive Fulde-Ferrel-Larkin-Ovchinikov superconducting state.[9] In all these interfaces, the conducting layers extend several monolayers into the bulk and consist of multiple subbands,[10] making them complicated quasi-2D materials. On the other hand, there has been considerable interest[11] on the 5d materials in the last few years such as Sr_2IrO_4 (SIO) on account of the large spin-orbit coupling that controls their electronic behavior, and recently experimenters have been able to grow interfaces between 3d and 5d oxides,[12–15] including those between LAO and SIO, the subject of this paper.

In this paper, based on density-functional studies, we predict a sharply localized 2DEG at the (001) LAO/SIO interface between 3d and 5d oxides, with properties fundamentally different from the 3d oxide interfaces studied to date, in the sense that: (i) The 2DEG is localized on a single IrO_2 monolayer at the interface, (ii) The 2DEG is spin-orbital entangled due to the strong spin-orbit coupling, and (iii) The interface electronic structure consists of a single half-filled band, leading to a simple model system for the spin-orbital entangled electron gas.

We studied this interface using density-functional theory (DFT) with the all-electron full-potential linear muffin-tin orbitals (FP-LMTO) method[16–19] including both the spin-orbit coupling (SOC) and Hubbard U terms in the local spin density approximation[20] (LSDA+SO+U). We used the supercell (001) $(LAO)_{5.5}/(SIO)_{4.5}$, where the half layers in the formula signify an extra layer of LaO and IrO_2, so that we have two identical interfaces (LaO/IrO_2) present in the supercell.

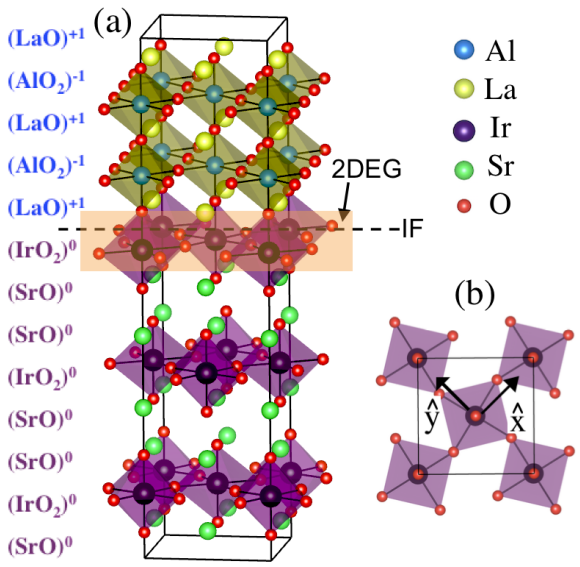

FIG. 1: (Color online) Structure of the n-type (001) LAO/SIO polar interface (IF) showing the corner-sharing IrO_6 and AlO_6 octahedra, the former with staggered rotations as indicated in (b). The nominal layer charges are indicated on the left. Electronic reconstruction due to the polar structure leads to a 2DEG, indicated by the yellow strip, which is spin-orbital entangled and sharply localized on a *single* IrO_2 plane.

The interface structure is shown in Fig. 1, where only a portion of the supercell is shown. The unit cell size in the *ab* plane was doubled ($\sqrt{2}a_0 \times \sqrt{2}a_0$) in order to accommodate the anti-ferromagnetic (AFM) structure of SIO, where a_0 is the in-plane Ir-Ir distance. The in-plane lattice constant of the interface structure was matched to the lattice constant of SIO, and the out-of-plane lattice constant for the LAO part was reduced to match its bulk experimental volume. The interface distance was optimized using pseudopotential method in the local-density approximation (LDA) as implemented in the Vienna *ab-initio* simulation package (VASP)[21,22]. Brillouin zone integrations were carried out by using a $8 \times 8 \times 1$ **k**-point mesh.

With the layers on the LAO side charged alternately

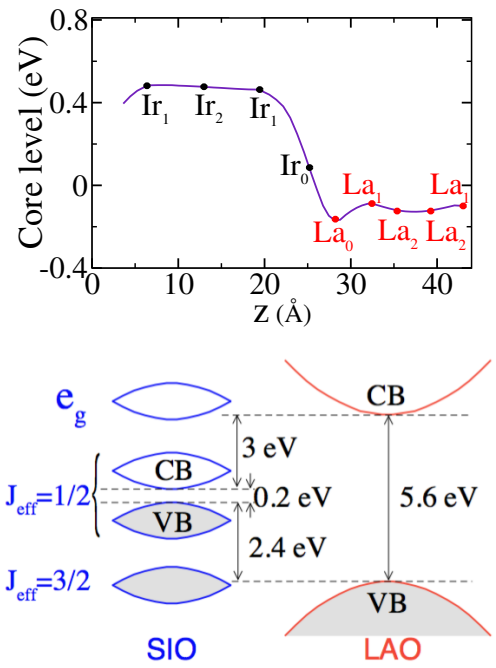

FIG. 2: (Color online) Oxygen 1s core level energy, averaged over the LAO or SIO formula unit, along direction, normal to the interface (*top*) and the calculated band-offset (*bottom*). The band alignment indicates that the added electrons reside in the $J_{\rm eff} = 1/2$ upper Hubbard band in the SIO part, which makes up the lowest conduction band. The interface Ir layer is denoted by $\rm Ir_0$, while $\rm Ir_1$ and $\rm Ir_2$ are the subsequent layers, and similar notations are adopted for the La layers as well, as indicated in the *top* figure.

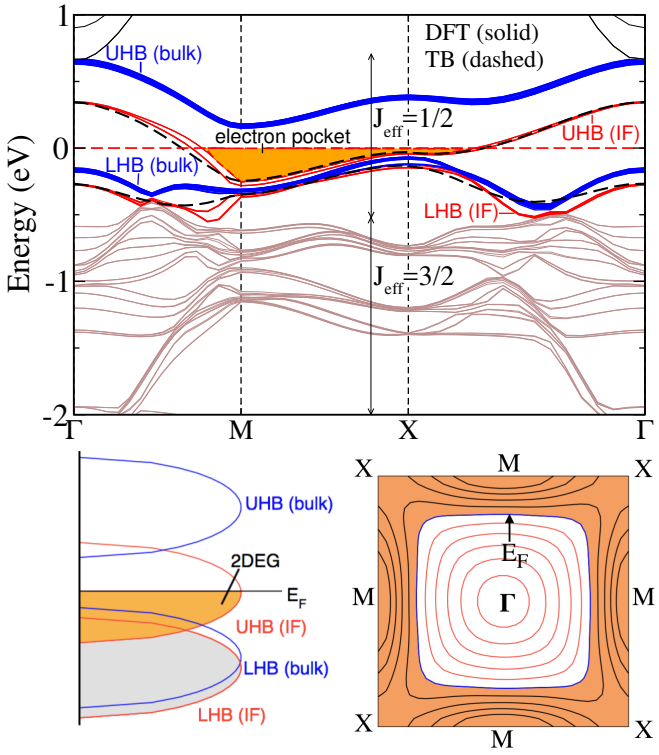

FIG. 3: (Color online) *Top*, Band structure of the LAO/SIO interface (IF) obtained from the FP-LMTO method with the LSDA+SO+U functional. Shown also are the tight-binding (TB) fit to the interface lower and upper Hubbard bands using the effective $J_{\rm eff} = 1/2$ model, Eq. (3). The symmetry points are: $\Gamma = (0,0)$, M$= \pi/2a_0(1,1)$, and X$= \pi/a_0(1,0)$, where $T_1 = a_0(1,1)$ and $T_2 = a_0(-1,1)$ are the primitive lattice translation vectors. The Fermi energy E_F is taken as zero. *Bottom left* shows the schematic electron states near E_F, all of $J_{\rm eff} = 1/2$ character, while the *bottom right* shows the square-like Fermi surface in the interface Brillouin zone with the hole pocket at Γ.

positive and negative and the SIO layers being neutral (Fig. 1), it is expected that the polar catastrophe[1,23] resulting from these nominal charges would lead to the accumulation of half an electron per Ir at the interface, making this an "n-type" interface.

The localization region of the accumulated electrons is determined by the band offset. To determine this, we have computed the band offset by: (i) Determining the positions of the valence band tops in the two constituent bulk materials with respect to the oxygen 1s core levels, (ii) Calculating the same core level energies in the supercell geometry, and finally (iii) Positioning the valence band tops on top of the supercell oxygen core level profile on either side of the interface, in the bulk regions away from the interface. Since DFT does not reproduce the band gaps very well, the experimental values of the band gaps were used to determine the conduction band offset, once the valence band offset has been calculated.

The calculated band offset is shown in Fig. 2. The figure indicates schematically the crystal-field splitting between the Ir t_{2g} and e_g states, the spin-orbit splitting of the t_{2g} into $J_{\rm eff} = 3/2$ and $1/2$ states, as well as the splitting of the $J_{\rm eff} = 1/2$ states into a lower and upper Hubbard band (LHB/UHB) due to the Coulomb interaction U, that leads to a Mott-Hubbard insulating state in the SIO bulk.[24] The band offset results clearly show that the $J_{\rm eff} = 1/2$ states, constituting the valence and conduction bands in SIO, lie well within the fundamental gap of LAO. This in turn indicates that the accumulated electrons at the interface would then reside in the $J_{\rm eff} = 1/2$ upper Hubbard band.

The band structure in the 2D interface Brillouin zone is shown in Fig. 3, which can be easily understood in terms of the bulk band structure of SIO. As already anticipated from the band offset results Fig. 2, the $J_{\rm eff} = 1/2$ orbitals form the bands around E_F, with the extra electrons at the interface (half per interface Ir atom) partially occupying the interface UHB, leading to a metallic interface. What is remarkable is that unlike the well-studied LAO/STO and many other 3d oxide interfaces, (i) the extra electron at the interface is confined to a single $\rm IrO_2$ layer and (ii) it occupies a single interfacial subband as opposed to multiple d bands. The spin-orbital entanglement of the bulk SIO continues to remain an interesting feature of the 2DEG as well. The electron states around

TABLE I: Calculated net electron charge (units of electron) on the Ir layers as well as the spin (μ_s) and orbital (μ_l) magnetic moments (units of μ_B). Ir_0 is the interface layer and Ir_1 and Ir_2 are the subsequent layers. The bulk behavior is obtained already for Ir_1, just one layer from the interface.

atom	Ir_0	Ir_1	Ir_2
charge	0.53	-0.01	-0.02
μ_s	0.02	0.36	0.36
μ_l	0.02	0.40	0.40

E_F are schematically shown in the bottom panel of Fig. (3), which also shows the square-like Fermi surface made up of the UHB of the interface Ir layer.

The magnetic moments calculated with DFT are sensitive to the choice of the Hubbard U parameter for Ir, yielding $m = 0.76\mu_B$ for $U = 3.4$ eV and $J = 0.7$ eV (present calculation), while $m = 0.36\mu_B$ for $U = 2$ eV[24], which bracket the measured value of $m = 0.5\mu_B$ from magnetic susceptibility.[25] While SIO is a canted AFM in the bulk, our calculations show that the interface IrO_2 layer is nearly non-magnetic, with only a very small net AFM magnetic moment of about $0.04\mu_B$ (Table I). Note that in the Dubarev approach[26], which we use in our LSDA+U calculations, only the combination $U_{\rm eff} = U - J = 2.7$ eV appears in the functional and not the individual parameters U and J. The computed magnetization profile is more or less the same as the bulk beyond the interfacial Ir_0 layer, indicating that the bulk behavior is quickly recovered away from the interface.

The $J_{\rm eff} = 1/2$ bands near E_F can be divided into two groups, viz., bulk like bands (shown in blue in Fig. (3)) and interface bands (shown in red), with the electron states in the latter more or less confined to a single IrO_2 layer at the interface. The energy dispersion of the bulk-like bands is nearly identical with the band structure of the constituent SIO bulk, while the interface bands are substantially different, with the LHB and UHB nearly collapsing along the M-X line of the Brillouin zone, which is due to a reduced staggered fiield Δ for the interface layer as discussed below.

The interface bands can be described by the 2D Hubbard model for the $J_{\rm eff} = 1/2$ bands on the square lattice, corresponding to a single anti-ferromagnetic IrO_2 layer since these layers are well separated. This model has been successfully used to describe the band structure of bulk SIO.[27,28] With $c^\dagger_{i\alpha}$ being the creation operator at site i (sublattice A or B) for the two $|J_{\rm eff}, m\rangle$ states, $|e_1\rangle \equiv |\frac{1}{2}, -\frac{1}{2}\rangle = (|xy\uparrow\rangle + |yz\downarrow\rangle + i|xz\downarrow\rangle)/\sqrt{3}, |e_2\rangle \equiv |\frac{1}{2}, \frac{1}{2}\rangle = (|yz\uparrow\rangle - i|xz\uparrow\rangle - |xy\downarrow\rangle)/\sqrt{3}$, the Hubbard model is

$$\mathcal{H} = \sum_{\langle ij\rangle\alpha} t_{ij} c^\dagger_{i\alpha} c_{j\alpha} + h.c. + \frac{U}{2}\sum_{i\alpha} n_{i\alpha} n_{i\bar{\alpha}}, \qquad (1)$$

where the hopping integral t_{ij} (in general complex due to the staggered rotations of the Ir octahedra) can be made real by a gauge transformation[29], U is the on-site Coulomb interaction, and the summation $\langle ij\rangle$ is over distinct pairs of neighbors.

The AFM lattice structure leads to a staggered field for the $|e_1\rangle$ and $|e_2\rangle$ orbitals, which do not mix. This leads to two identical 2×2 TB Hamiltonian in the momentum space for the $|e_1\rangle$ or $|e_2\rangle$ bands, viz.,

$$\mathcal{H}(\mathbf{k}) = \begin{pmatrix} -\Delta + h_{11} & h_{12} \\ h^*_{12} & \Delta + h_{11} \end{pmatrix}, \qquad (2)$$

where $h_{11} = 4t_2 \cos k_x \cos k_y + 2t_3(\cos 2k_x + \cos 2k_y)$, $h_{12} = 2t_1(\cos k_x + \cos k_y) + 4t_4(\cos 2k_x \cos k_y + \cos 2k_y \cos k_x)$, $a_0 = 1$ is the lattice constant, and $\Delta = U/2 \times (n_2 - n_1)$ is the Hartree-Fock staggered field, n_α being the occupancy of the $|e_\alpha\rangle$ orbitals. Diagonalization yields the TB band structure

$$\varepsilon_\pm(\mathbf{k}) = h_{11}(\mathbf{k}) \pm \sqrt{\Delta^2 + h^2_{12}(\mathbf{k})}. \qquad (3)$$

For bulk SIO, the TB parameters are:[27,30] $U = 0.65$, $t_1 = -0.095$, $t_2 = 0.015$, $t_3 = 0.035$, and $t_4 = 0.01$, all in units of eV. For the interface bands, a better fitting to the DFT bands is obtained with a significantly reduced value $U \approx 0.2$ eV, which may be due to enhanced electron screening because of the presence of the 2DEG. The condition for the conduction bottom to occur at the M point, $t_3 > t_2/2 > -t_1^2/(2\Delta)$, is easily satisfied, and the axis ratio of the elliptical contours around the M point is $r = [(2t_3 - t_2)/(t_2 + 2t_3 + 2\Delta^{-1}(t_1 - 2t_4)^2)]^{1/2} \approx 0.3$ for the interface bands. This explains the strongly anisotropic energy surface around M in Fig. (3).

The TB bands (Eq. 3) originating from the interface layer are shown by the dotted lines in Fig. (3). Because of the reduced U and the fact that the interface $J_{\rm eff} = 1/2$ states are three-quarters full, while the bulk states are only half full (LHB is full and UHB is empty), which reduces the staggered field $\Delta = (U/2)(n_2 - n_1)$, the interface bands have somewhat different dispersions from the bulk bands and they occur in the middle of the bulk band gap. In Fig. (3), there are two bands crossing E_F, which correspond to the two interfacial Ir_0 atoms in the unit cell. These atoms are not identical due to their slightly different magnetic moments in the calculation, leading to two bands which are slightly separated in energy. For a truly AFM structure, these two bands would be degenerate.

The Fermi surface is nearly square as shown in the bottom part of Fig. (3) with significant nesting, which could lead to charge or spin density instabilities, and possibly to the recently predicted nematic phases.[31] Study of these instabilities remains an open question both theoretically and experimentally.

To visualize the nature of the interface bands at the Fermi surface, we have plotted in Fig. 4 the charge and spin densities of the $J_{\rm eff} = 1/2$ states crossing E_F. As the figure shows, the extra electrons are sharply localized on the single interfacial Ir_0 layer and are spin-mixed as expected for the $J_{\rm eff} = 1/2$ band. The calculated total layer

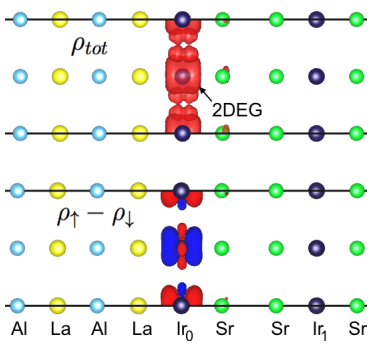

FIG. 4: (Color online) Total charge (*top*) and spin density difference (*bottom*) contours, corresponding to the 2DEG pocket shown in orange in Fig. 3. The 2DEG is sharply localized on more or less a single IrO_2 layer. Blue and red colors in the bottom panel correspond to opposite spin densities, indicating the spin-orbital entanglement.

charge is shown in Table I, which again shows the complete localization of the half electron on the single interfacial layer. This is very different from the 3d perovskite interfaces such as the much studied (001) LAO/STO interface, where the extra 1/2 electron at the interface is quite delocalized, extending several unit cells into the bulk.[10] Furthermore, the computed spin and orbital magnetic moments indicate that the bulk limit is quickly reached, almost immediately beyond the interfacial layer.

The layer projected partial densities of states (PDOS) are shown in Fig. 5, which are again consistent with the band offset results. The LAO states lie away from E_F except for a small admixture from the LaO layer adjacent to the interface. The small band gap between the UHB and the LHB within the $J_{\rm eff} = 1/2$ manifold of bulk SIO is apparent in the Ir_1 and Ir_2 PDOS, which have already reached the bulk limit. Integrating the $J_{\rm eff} = 1/2$ hole state in the Ir_0 panel above E_F, we find that there are 0.5 holes in this layer, consistent with the total layer charge density shown in Table I.

In summary, we have proposed a spin-orbital entangled 2DEG at the polar interface between a 5d and a 3d oxide material, a structure that is experimentally accessible. A very interesting property of the 2DEG is that it is sharply localized to a single 2D IrO_2 layer unlike the oxide interfaces studied to date such as the (001) LAO/STO interface, where the electron gas extends several layers into the bulk. Additionally, the interface has a simple band structure devoid of multiple subbands, which leads to a nested square-like Fermi surface. Our work suggests a novel, spin-orbital entangled 2DEG system that is experimentally accessible and may serve as a host for potentially exotic phases hitherto unknown, such as the recently predicted nematic phase[31].

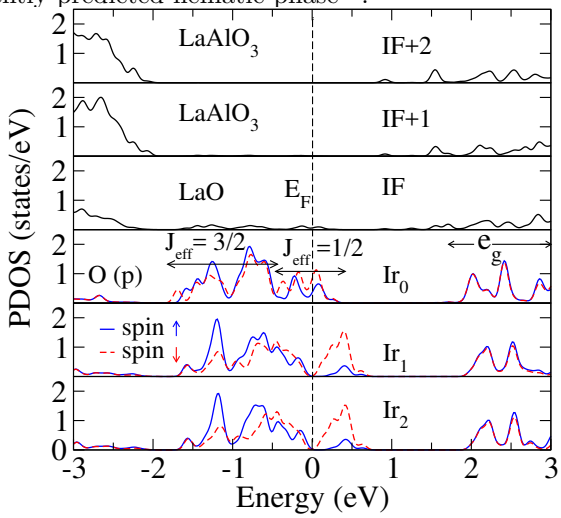

FIG. 5: (Color online) Layer resolved partial density of states in layers adjacent to the interface. Ir_0, Ir_1, and Ir_2 are iridium atoms in the IrO_2 planes with increasing distances from the interface.

Acknowledgments

We thank the U.S. Department of Energy, Office of Basic Energy Sciences, Division of Materials Sciences and Engineering (Grant No. DE-FG02-00ER45818) for financial support. Computational resources were provided by the National Energy Research Scientific Computing Center, a user facility also supported by the U.S. Department of Energy.

[1] A. Ohtomo and H. Y. Hwang, A high-mobility electron gas at the $LaAlO_3/SrTiO_3$ heterointerface, Nature **427**, 423 (2004).
[2] M. Diez, A. M. R. V. L. Monteiro, G. Mattoni, E. Cobanera, T. Hyart, E. Mulazimoglu, N. Bovenzi, C. W. J. Beenakker, and A. D. Caviglia, Giant negative magnetoresistance driven by spin-orbit coupling at the $LaAlO_3/SrTiO_3$ interface, Phys. Rev. Lett. **115**, 016803 (2015).
[3] B. R. K. Nanda, S. Satpathy, and M. Springborg, Electron leakage and double-exchange ferromagnetism at the interface between a metal and an antiferromagnetic insulator: $CaRuO_3/CaMnO_3$, Phys. Rev. Lett. **98**, 216804 (2007).
[4] A. D. Caviglia, S. Gariglio, N. Reyren, D. Jaccard, T. Schneider, M. Gabay, S. Thiel, G. Hammerl, J. Mannhart, and J.-M. Triscone, Electric field control of the $LaAlO_3/SrTiO_3$ interface ground state, Nature **456**, 624 (2008).
[5] A. D. Caviglia, M. Gabay, S. Gariglio, N. Reyren, C. Cancellieri, and J.-M. Triscone Tunable Rashba Spin-Orbit Interaction at Oxide Interfaces, Phys. Rev. Lett. **104**, 126803 (2010).
[6] A. Brinkman, M. Huijben, M. van Zalk, J. Huijben, U. Zeitler, J.C. Maan, W. G. van der Wiel, G. Rijnders, D.

H. A. Blank, and H. Hilgenkamp, Magnetic effects at the interface between non-magnetic oxides, Nat. Mater. **6**, 493 (2007).

[7] N. Reyren, S. Thiel, A. D. Caviglia, L. Fitting Kourkoutis, G. Hammerl, C. Richter, C. W. Schneider, T. Kopp, A.-S. Retschi, D. Jaccard, M. Gabay, D. A. Muller, J.-M. Triscone, and J. Mannhart Superconducting Interfaces Between Insulating Oxides, Science **317**, 1196 (2007).

[8] L. Fidkowski, H.-C. Jiang, R. M. Lutchyn, and C. Nayak, Magnetic and superconducting ordering in 1D nanostructures at the $LaAlO_3/SrTiO_3$ interface, Phys. Rev. B **87**, 014436 (2013).

[9] K. Michaeli, A. C. Potter, and P. A. Lee, Superconductivity and ferromagnetic phases in $SrTiO_3/LaAlO_3$ oxide interface structures: Possibility of finite momentum pairing, Phys. Rev. Lett. **108**, 117003 (2012).

[10] Z. S. Popović, S. Satpathy, and R. M. Martin, Origin of the Two-Dimensional Electron Gas Carrier Density at the LaAlO3 on SrTiO3 Interface, Phys. Rev. Lett. **101**, 256801 (2008).

[11] For a recent review, see, e. g., G. Cao and P. Schlottmann, "The challenge of spin-orbit-tuned ground states in iridates: a key issue review, Rep. Prog. Phys. **81**, 042502 (2018).

[12] J. Nichols, J. Terzic, E. G. Bittle, O. B. Korneta, L. E. De Long, J. W. Brill, G. Cao, and S. S. A. Seo, Tuning electronic structure via epitaxial strain in Sr_2IrO_4 thin films, Applied Physics Letters **102**, 141908 (2013).

[13] C. R. Serrao, J. Liu, J. T. Heron, G. Singh- Bhalla, A. Yadav, S. J. Suresha, R. J. Paull, D. Yi, J. -H. Chu, M. Trassin, A. Vishwanath, E. Arenholz, C. Frontera, J. Zelezny, T. Jungwirth, X. Marti, and R. Ramesh, Epitaxy-distorted spin-orbit Mott insulator in Sr_2IrO_4 thin films, Phys. Rev. B **87**, 085121 (2013).

[14] J. Nichols, X. Gao, S. Lee, T. L. Meyer, J. W. Freeland, V. Lauter , D. Yi, J. Liu, D. Haskel, J. R. Petrie, E.-J. Guo, A. Herklotz, D. Lee, T. Z. Ward, G.Eres, M. R. Fitzsimmons, and H. N. Lee, Emerging magnetism and anomalous Hall effect in iridate-manganite heterostructures, Nat. Comm. **7**, 12721 (2016).

[15] E. J. Moon, A. F. May, P. Shafer, E. Arenholz, and S. J. May, Growth and electrical transport properties of $La_{0.7}Sr_{0.3}MnO_3$ thin films on Sr_2IrO_4 single crystals, Phys. Rev. B **95**, 155135 (2017).

[16] O. K Andersen, Linear methods in band theory, Phys. Rev. B **12**, 3060 (1975).

[17] M. Methfessel and M. van Schilfgaarde and R.A. Casali, A Full-Potential LMTO Method Based on Smooth Hankel Functions, Electronic Structure and Physical Properties of Solids. The Use of the LMTO Method, Lecture Notes in Physics **535**, 114 (2000).

[18] T. Kotani and M. van Schilfgaarde, Fusion of the LAPW and LMTO methods: The augmented plane wave plus muffin-tin orbital method, Phys. Rev. B **81**, 125117 (2010).

[19] See https://www.questaal.org.

[20] U. von Barth and L. Hedin, A local exchange-correlation potential for the spin polarized case. i, Journal of Physics C: Solid State Physics **5**, 1629 (1972).

[21] G. Kresse and J. Furthmüller, Efficient iterative schemes for ab initio total-energy calculations using a plane-wave basis set, Phys. Rev. B **54**, 11169 (1996).

[22] G. Kresse and D. Joubert, From ultrasoft pseudopotentials to the projector augmented-wave method, Phys. Rev. B **59**, 1758 (1999).

[23] W. A. Harrison, E. A. Kraut, J. R. Waldrop, and R. W. Grant, Polar heterojunction interfaces, Phys. Rev. B **18**, 4402 (1978).

[24] B. J. Kim, H. Jin, S. J. Moon, J.-Y. Kim, B.-G. Park, C. S. Leem, J. Yu, T. W. Noh, C. Kim, S.-J. Oh, J.-H. Park, V. Durairaj, G. Cao, and E. Rotenberg, Novel $J_{\rm eff} = 1/2$ Mott State Induced by Relativistic Spin-Orbit Coupling in Sr_2IrO_4, Phys. Rev. Lett. **101**, 076402 (2008).

[25] G. Cao, J. Bolivar, S. McCall, J. E. Crow, and R. P. Guertin, Weak ferromagnetism, metal-to-nonmetal transition, and negative differential resistivity in single-crystal Sr_2IrO_4, Phys. Rev. B **57**, R11039 (1998).

[26] S. L. Dubarev, G. A. Botton, S. Y. Savrasov, C. J. Humphreys, and A. P. Sutton, Electron-energy-loss spectra and the structural stability of nickel oxide: An LSDA+U study, Phys. Rev. B **57**, 1505 (1998).

[27] C. Bhandari, Z. S. Popović, and S. Satpathy, Electronic structure and optical properties of Sr_2IrO_4 under epitaxial strain, ArXiv:1802.09719 (2018).

[28] H. Watanabe, T. Shirakawa, and S. Yunoki, Microscopic study of a spin-orbit-induced Mott insulator in Ir oxides, Phys. Rev. Letts. **105**, 216410 (2010).

[29] S. Mohapatra, J. van den Brink, and A. Singh, Magnetic excitations in a three-orbital model for the strongly spin-orbit coupled iridates: Effect of mixing between the $J = 1/2$ and $3/2$ sectors, Phys. Rev. B **95**, 094435 (2017).

[30] S. Bhowal, J. Moradi Kurdestany, and S. Satpathy, Stability of the Antiferromagnetic State in the Electron Doped Iridates, J. Phys: Cond. Mat. **30**, 235601 (2018).

[31] N. Boudjada, G. Wachtel, and A. Paramekanti, Magnetic and nematic orders of the 2DEG ai oxide (111) surfaces and interfaces, Phys. Rev. Lett. **120**, 086802 (2018).